Post-transcriptional repression of mRNA enhances competence to transit from mitosis to meiosis in mouse spermatogenic cells

Maria M. Mikedis[a,b,c,1], Bingrun Liu[c], Dirk G. de Rooij[c], and David C. Page[c,d,e]

[a] Reproductive Sciences Center, Division of Developmental Biology, Cincinnati Children's Hospital Medical Center, Cincinnati, OH, United States

[b] Department of Pediatrics, University of Cincinnati College of Medicine, Cincinnati, OH United States

[c] Whitehead Institute, Cambridge, MA, United States

[d] Department of Biology, Massachusetts Institute of Technology, Cambridge, MA, United States

[e] Howard Hughes Medical Institute, Whitehead Institute, Cambridge, MA, United States

[1] Correspondence should be addressed to M.M.M. (maria.mikedis@cchmc.org)

ABSTRACT

The special cell cycle known as meiosis transforms diploid germ cells into haploid gametes. In mammalian testes, diploid spermatogenic cells become competent to transition from mitosis to meiosis in response to retinoic acid. In mice, previous studies revealed that MEIOC, alongside binding partners YTHDC2 and RBM46, represses mitotic genes and promotes robust meiotic gene expression in spermatogenic cells that have already initiated meiosis. Here, we molecularly dissect MEIOC-dependent regulation in mouse spermatogenic cells and find that MEIOC actually shapes the transcriptome much earlier, even before meiotic initiation. MEIOC, acting with YTHDC2 and RBM46, destabilizes mRNA targets, including transcriptional repressors *E2f6* and *Mga*, in mitotic spermatogonia. MEIOC thereby derepresses E2F6- and MGA-repressed genes, including *Meiosin* and other meiosis-associated genes. This confers on spermatogenic cells the molecular competence to, in response to retinoic acid, fully activate the STRA8-MEIOSIN transcriptional regulator, which is required for the meiotic G1/S cell cycle transition and meiotic gene expression. We conclude that in mice, mRNA decay mediated by MEIOC-YTHDC2-RBM46 enhances the competence of mitotic spermatogonia to transit from mitosis to meiosis.

18 **INTRODUCTION**

19 Sexual reproduction depends on meiosis – a specialized cell cycle that produces haploid gametes
20 via one round of DNA replication followed by two rounds of chromosome segregation. The
21 major chromosomal events of meiosis, including pairing, synapsis, and crossing over of
22 homologous chromosomes, are generally conserved across eukaryotes. By contrast, the
23 mechanisms that govern the transition from mitosis to meiosis are less well conserved (Kimble
24 2011). For example, in budding yeast, meiotic initiation occurs when multiple inputs converge to
25 activate a master transcription factor (IME1) that upregulates meiotic gene expression (reviewed
26 in van Werven and Amon 2011; Kassir et al. 1988; Smith et al. 1990). In *Drosophila*
27 *melanogaster*, the transition from mitosis to meiosis occurs via translational repression mediated
28 by the RNA helicase Bgcn and its binding partner Bam (Gonczy et al. 1997; McKearin and
29 Spradling 1990; Chen et al. 2014; Insco et al. 2009, 2012).

30 In mammals, transcriptional activation induced by extrinsic signaling plays a central role
31 in the mitosis-to-meiosis (i.e., meiotic G1/S) transition. Retinoic acid induces meiotic entry by
32 activating the gene expression of *Stra8* and *Meiosin* (Baltus et al. 2006; Anderson et al. 2008a;
33 Dokshin et al. 2013; Ishiguro et al. 2020). Acting as a heterodimer, STRA8-MEIOSIN
34 transcriptionally activates the robust expression of G1/S cyclins as well as meiotic factors that
35 orchestrate the chromosomal events of meiotic prophase I (Baltus et al. 2006; Anderson et al.
36 2008a; Soh et al. 2015; Kojima et al. 2019; Ishiguro et al. 2020; Mark et al. 2008). In mice on a
37 C57BL/6 genetic background, premeiotic oocytes and preleptotene spermatocytes with *Stra8* or
38 *Meiosin* genetically ablated halt development and fail to progress into meiotic prophase I
39 (Anderson et al. 2008a; Baltus et al. 2006; Dokshin et al. 2013; Ishiguro et al. 2020). In addition,

40 *Stra8*-null premeiotic oocytes and preleptotene spermatocytes fail to undergo meiotic DNA
41 replication (Anderson et al. 2008a; Baltus et al. 2006; Dokshin et al. 2013).
42 In the mammalian testis, competence to transit from mitosis to meiosis in response to
43 retinoic acid is acquired during spermatogenesis. In mitotic spermatogonia, DMRT1 postpones
44 the acquisition of competence, thereby preventing precocious meiotic entry, by repressing
45 retinoic acid-dependent transcription as well as *Stra8* and likely *Meiosin* gene expression
46 (Matson et al. 2010; Ishiguro et al. 2020). As a result, undifferentiated spermatogonia exposed to
47 endogenous retinoic acid express low levels *Stra8*, but do not express *Meiosin*, and consequently
48 become mitotic differentiating spermatogonia (Matson et al. 2010; Ishiguro et al. 2020).
49 Differentiating spermatogonia prematurely exposed to exogenous retinoic acid may express
50 STRA8 protein, but they do not initiate meiosis (Johnson et al. 2023; Endo et al. 2015). At the
51 mitosis-to-meiosis transition, the SCF E3 ubiquitin ligase complex degrades DMRT1 (Matson et
52 al. 2010; Nakagawa et al. 2017), thereby conferring upon spermatogenic cells the competence to
53 express *Stra8* and *Meiosin* and initiate meiosis in response to retinoic acid. To date, the SCF
54 complex is the only known positive regulator of the spermatogenic cells' competence to transit
55 from mitosis to meiosis in response to retinoic acid.
56 Post-transcriptional regulation of mRNA plays a role in governing early meiotic prophase
57 I in mammals. MEIOC acts together with RNA helicase YTHDC2 and RNA-binding protein
58 RBM46 to regulate entry into and progression through meiotic prophase I (Abby et al. 2016; Soh
59 et al. 2017; Wojtas et al. 2017; Bailey et al. 2017; Hsu et al. 2017; Jain et al. 2018; Qian et al.
60 2022). During meiotic prophase I, MEIOC is required to increase meiotic gene expression and
61 repress the mitotic cell cycle program, with the latter of these two functions inhibiting a
62 premature and aberrant metaphase several days before wild-type meiotic metaphase I. Consistent

63 with MEIOC's distant homology to Bam and YTHDC2's homology to Bgcn, the MEIOC-
64 YTHDC2-RBM46 complex binds to mRNA (Hsu et al. 2017; Soh et al. 2017; Abby et al. 2016;
65 Bailey et al. 2017; Li et al. 2022; Saito et al. 2022; Jain et al. 2018). YTHDC2 interacts with
66 exoribonuclease XRN1, while RBM46 recruits UPF1, a mediator of nonsense mediated decay,
67 and subunits of the cytoplasmic deadenylase CCR4-NOT complex, which suggests that
68 YTHDC2 and RBM46's mRNA targets are degraded (Wojtas et al. 2017; Li et al. 2022; Qian et
69 al. 2022; Kretschmer et al. 2018). However, how the MEIOC-YTHDC2-RBM46 complex post-
70 transcriptionally regulates its mRNA targets during entry into meiotic prophase I remains poorly
71 defined.

72 Here we molecularly dissect MEIOC's activity in mouse spermatogenic cells during the
73 mitosis-to-meiosis transition via two parallel approaches: (i) single-cell RNA sequencing
74 (scRNA-seq) analysis of postnatal testes and (ii) bulk RNA-seq analysis of developmentally
75 synchronized testes with histologically verified staging. Both approaches reveal that *Meioc*-null
76 germ cells developmentally diverge from wild-type spermatogenic cells at the meiotic G1/S
77 transition, earlier than previously appreciated. Furthermore, we find that MEIOC's activity leads
78 to an increase in meiosis-associated gene expression in late mitotic spermatogonia, before
79 meiotic initiation. We discover that MEIOC destabilizes mRNAs encoding transcriptional
80 repressors of meiotic gene expression. This repression of repressors facilitates activation of the
81 master meiotic transcriptional regulator STRA8-MEIOSIN in response to retinoic acid.
82 Therefore, a post-transcriptional repressor of mRNA, acting in parallel to the SCF complex's
83 degradation of DMRT1, enhances spermatogenic cells' competence to activate the meiotic
84 transcriptional regulator and transition from mitosis to meiosis.

85 **RESULTS**

86 **MEIOC's activity facilitates a major transcriptomic shift at the meiotic G1/S transition**

87 To characterize the molecular consequences of MEIOC activity on spermatogenesis, we
88 performed 10x Genomics Chromium-based scRNA-seq on *Meioc*-null and wild-type P15 testes
89 and identified germ cell clusters by cell type-enriched marker expression and transcriptome-
90 based cell cycle analysis (Fig. S1-3; Supplemental Information). These germ cell clusters
91 consisted of four clusters in mitosis (undifferentiated spermatogonia [Undiff], differentiating
92 types A_1-A_4 spermatogonia [A1-4], differentiating Intermediate and type B spermatogonia
93 [In/B], and differentiating type B spermatogonia in G2/M phase [B G2M]); three clusters
94 spanning the mitosis-to-meiosis transition (preleptotene spermatocytes in G1, early S, and late S
95 phase [pL G1, pL eS, and pL lS, respectively]); and three clusters in meiotic prophase I
96 (leptotene spermatocytes [L], zygotene spermatocytes [Z], and pachytene spermatocytes [P]).

97 We then applied pseudotime analysis to reconstruct the germ cells' developmental
98 trajectory from undifferentiated spermatogonia to pachytene spermatocytes (Fig. 1A). *Meioc*-null
99 germ cells followed the same trajectory as wild-type cells during the mitotic stages of
100 spermatogenesis but diverged in the G1 phase of the preleptotene stage, just before meiotic S
101 phase begins. We used bulk RNA-seq analysis of testes developmentally synchronized and
102 histologically verified for preleptotene spermatocytes to confirm that MEIOC is associated with
103 transcriptomic changes at this stage, including increased abundance of G1/S transcripts (Fig.
104 S4A-D; Supplemental Information). This demonstrates that MEIOC drives a major
105 transcriptomic shift in spermatogenic cells at the meiotic G1/S transition.

106

Figure 1

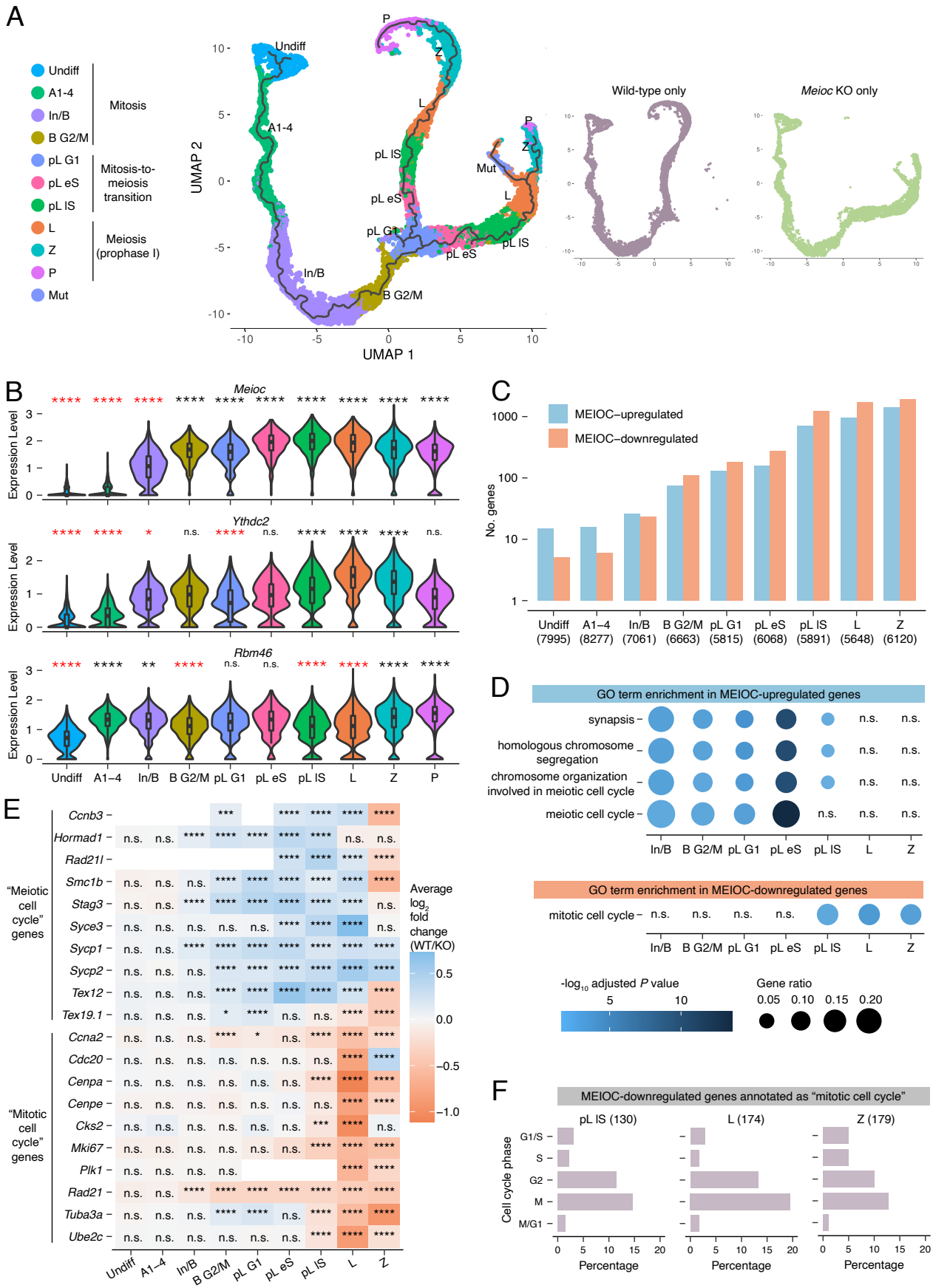
A
Undiff
A1-4
In/B
B G2/M
pL G1
pL eS
pL IS
L
Z
P
Mut
Mitosis
Mitosis-to-meiosis transition
Meiosis (prophase I)
UMAP 1
UMAP 2
Wild-type only
Meioc KO only
B
Meioc
Ythdc2
Rbm46
Expression Level
Undiff
A1–4
In/B
B G2/M
pL G1
pL eS
pL IS
L
Z
P
C
MEIOC–upregulated
MEIOC–downregulated
No. genes
Undiff (7995)
A1–4 (8277)
In/B (7061)
B G2/M (6663)
pL G1 (5815)
pL eS (6068)
pL IS (5891)
L (5648)
Z (6120)
D
GO term enrichment in MEIOC-upregulated genes
synapsis
homologous chromosome segregation
chromosome organization involved in meiotic cell cycle
meiotic cell cycle
GO term enrichment in MEIOC-downregulated genes
mitotic cell cycle
-log10 adjusted P value
Gene ratio
E
"Meiotic cell cycle" genes
"Mitotic cell cycle" genes
Ccnb3
Hormad1
Rad21l
Smc1b
Stag3
Syce3
Sycp1
Sycp2
Tex12
Tex19.1
Ccna2
Cdc20
Cenpa
Cenpe
Cks2
Mki67
Plk1
Rad21
Tuba3a
Ube2c
Average log2 fold change (WT/KO)
F
MEIOC-downregulated genes annotated as "mitotic cell cycle"
pL IS (130)
L (174)
Z (179)
Cell cycle phase
G1/S
S
G2
M
M/G1
Percentage

Figure 1: *Meioc*-null germ cells transcriptomically diverge from wild-type germ cells during the G1/S phase transition.

A: UMAP visualization with pseudotime trajectory of wild-type and *Meioc* KO germ cells from P15 testes. Large plot on left displays both wild-type and *Meioc* KO cells. Smaller plots on right display cells of a single genotype.

B: Expression levels of *Meioc*, *Ythdc2*, and *Rbm46* in germ cell clusters from wild-type testes. Black and red asterisks designate enrichment or depletion, respectively, relative to all other germ cells. Clusters marked as “not done” (n.d.) did not meet expression thresholds set for statistical testing.

C: Number of genes identified as MEIOC-upregulated ($\log_2$ fold change (WT/KO)>0.1, adj. P<0.05) and -downregulated ($\log_2$ fold change (WT/KO)<-0.1, adj. P<0.05) within each germ cell cluster.

D: Gene Ontology (GO) term enrichment analysis for MEIOC-upregulated and -downregulated genes shown. Graph for MEIOC-upregulated genes displays top 4 enriched categories identified in the B G2/M cluster. Graph for MEIOC-downregulated genes displays a selected category of interest.

E: Heatmap of $\log_2$ fold changes for selected genes annotated as GO terms “meiotic cell cycle” or “mitotic cell cycle”.

F: Associated cell cycle phases for MEIOC-downregulated genes that are annotated as GO term “mitotic cell cycle.” Only those genes whose expression is associated with a specific cell cycle phase are graphed.

Cluster abbreviations: Undiff, undifferentiated spermatogonia; A1-4, differentiating types A_1-A_4 spermatogonia; In/B, differentiating Intermediate and type B spermatogonia; B G2M, differentiating type B spermatogonia in G2/M phase; pL G1, preleptotene spermatocytes in G1 phase; pL eS, preleptotene spermatocytes in early S; pL lS, preleptotene spermatocytes in late S phase; L, leptotene spermatocytes; Z, zygotene spermatocytes; P, pachytene spermatocytes; Mut, mutant spermatocytes.

*, adj. P<0.05; **, adj. P<0.01; ***, adj. P<0.001; ****, adj. P<0.0001; n.s., not significant.

107 **MEIOC predominantly affects the abundance of meiotic, rather than mitotic, transcripts**
108 **before the meiotic G1/S transition**

109 MEIOC protein is first detected immunohistochemically at the preleptotene stage (Soh et al.
110 2017; Abby et al. 2016). We found that *Meioc* transcripts became highly abundant at an earlier
111 stage, in late mitotic spermatogonia (In/B and B G2M clusters) (Fig. 1B). Binding partner *Ythdc2*
112 followed a similar pattern of expression, while *Rbm46* was highly abundant in all germ cell
113 clusters examined. These observations raised the possibility that MEIOC, potentially in
114 collaboration with YTHDC2 and RBM46, shapes the germline transcriptome in late mitotic
115 spermatogonia, before the protein can be reliably detected via immunostaining.

116 To assess how MEIOC impacts the transcriptome during spermatogenesis, we carried out
117 scRNA-seq-based differential expression analysis in germ cell clusters associated with mitotic
118 spermatogonia (Undiff, A1-4, In/B, and B G2M clusters), the mitosis-to-meiosis transition (pL
119 G1, eS, and lS clusters), and meiotic prophase I (L and Z clusters), and identified genes whose
120 transcript abundance is upregulated ($\log_2$ fold change WT/*Meioc* KO > 0.1 and adjusted $P <$
121 0.05) or downregulated ($\log_2$ fold change WT/*Meioc* KO < -0.1 and adjusted $P < 0.05$) (Fig. 1C)
122 by MEIOC. The number of differentially abundant transcripts increased in the In/B and B G2/M
123 clusters, mirroring *Meioc* and *Ythdc2* expression patterns, and continued to expand thereafter.
124 We conclude that MEIOC affects the germline transcriptome before the meiotic G1/S transition.

125 Based on functional analysis, transcripts upregulated by MEIOC in the In/B through L
126 clusters were enriched for annotations related to meiosis (Fig. 1D). Several transcripts
127 contributing to this enrichment became more abundant in mitotic spermatogonia and remained
128 more abundant in early meiotic spermatocytes (Fig. 1E). Bulk RNA-seq analysis of preleptotene-
129 enriched testes also revealed enrichment of meiosis-associated factors among MEIOC-

130 upregulated transcripts (Fig. S4C, E). Therefore, MEIOC's activity leads to increased meiotic
131 transcript abundance in late mitotic spermatogonia, earlier than previously appreciated.
132 Given that MEIOC decreases mitotic transcript abundance in P10 testes (Soh et al. 2017),
133 we asked whether these transcriptomic changes were also induced by MEIOC in mitotic
134 spermatogonia. MEIOC-downregulated transcripts were enriched in "mitotic cell cycle" factors
135 in the pL lS to Z clusters but not in developmentally earlier clusters (Fig. 1D,E). Furthermore,
136 based on a curated list of genes whose expression is linked to specific cell cycle phases (Hsiao et
137 al. 2020), these MEIOC-downregulated "mitotic cell cycle" genes were primarily associated with
138 G2 or M phases (Fig. 1F). Therefore, the downregulation of "mitotic cell cycle" transcripts
139 occurs primarily after the meiotic G1/S transition and is consistent with MEIOC preventing an
140 aberrant M phase during meiotic prophase I.
141 In sum, MEIOC increases the abundance of meiosis-associated transcripts beginning in
142 late transit-amplifying spermatogonia. Only later in the mitosis-to-meiosis transition does
143 MEIOC decrease mitotic transcript abundance.
144
145 **MEIOC destabilizes its target transcripts**
146 In early spermatocytes, MEIOC localizes to the cytoplasm and interacts with RNA-binding
147 proteins YTHDC2 and RBM46, which recruit additional proteins that degrade mRNA (Wojtas et
148 al. 2017; Li et al. 2022; Qian et al. 2022; Kretschmer et al. 2018). Therefore, we hypothesized
149 that MEIOC degrades its mRNA targets. We first defined transcripts that associate with MEIOC
150 by reanalyzing our previously published MEIOC RIP-seq data from P15 testes (Soh et al. 2017),
151 identifying 1,991 MEIOC-bound mRNA targets. We then assessed the molecular impact of
152 MEIOC's interaction with these transcripts via two approaches. First, we examined these targets'

153 representation among transcripts exhibiting statistically significant MEIOC-dependent changes
154 in abundance. We found that MEIOC targets were enriched among transcripts whose abundance
155 decreased, but not increased, in response to MEIOC, in the B G2/M through Z clusters (Fig. 2A).
156 Second, we examined all MEIOC targets as a group, irrespective of whether they met a statistical
157 cut off in the differential expression analysis. MEIOC targets exhibited slightly lower fold
158 changes (WT/KO) than nontargets in the A1-4 through Z clusters (Fig. 2B). A parallel analysis
159 of computationally estimated changes in transcript stability from bulk RNA-seq data showed that
160 MEIOC targets had reduced transcript stability relative to nontargets (Fig. S6A). Therefore,
161 MEIOC decreases the abundance of its target transcripts, presumably by promoting post-
162 transcriptional degradation, beginning in mitotic spermatogonia, before the mitosis-to-meiosis
163 transition.

164 Given MEIOC's interaction with YTHDC2 and RBM46, we hypothesized that many
165 MEIOC targets are also bound by YTHDC2 and RBM46. Based on recently published YTHDC2
166 and RBM46 CLIP data from the testis (Saito et al. 2022; Qian et al. 2022), MEIOC shared 202
167 mRNA targets with YTHDC2 and 1,477 targets with RBM46, both of which are statistically
168 significant overlaps (Fig. 2C). All three proteins shared 187 targets. Only 15 mRNAs were
169 bound by MEIOC and YTHDC2 but not RBM46; this small group likely represents technical
170 differences between datasets rather than a biologically meaningful set of transcripts. We
171 conclude that MEIOC shares many, but not all, of its mRNA targets with YTHDC2 and RBM46.

172 As YTHDC2 and RBM46 interact with proteins that degrade mRNA, we hypothesized
173 that MEIOC's interaction with YTHDC2 and RBM46 has a greater impact on transcript stability
174 than MEIOC alone. We subsequently binned MEIOC's targets as: MEIOC-RBM46-YTHDC2
175 targets, MEIOC-RBM46-only targets, MEIOC-YTHDC2-only, and MEIOC-only targets. We

Figure 2

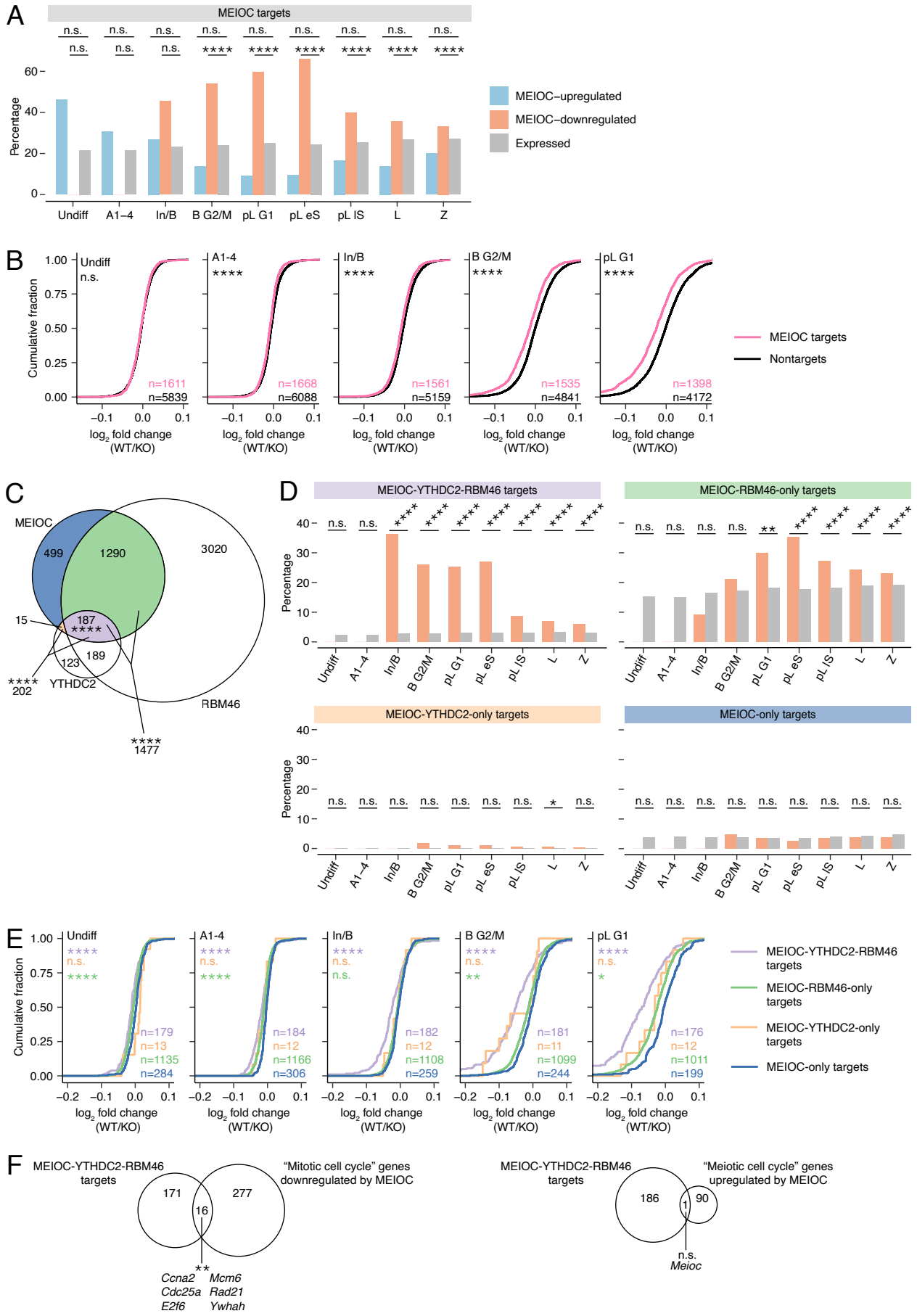
A
MEIOC targets
Percentage
MEIOC–upregulated
MEIOC–downregulated
Expressed
Undiff
A1–4
In/B
B G2/M
pL G1
pL eS
pL lS
L
Z
B
Cumulative fraction
log2 fold change (WT/KO)
MEIOC targets
Nontargets
n=1611
n=5839
n=1668
n=6088
n=1561
n=5159
n=1535
n=4841
n=1398
n=4172
C
MEIOC
499
1290
3020
15
187
189
123
YTHDC2
RBM46
202
1477
D
MEIOC-YTHDC2-RBM46 targets
MEIOC-RBM46-only targets
MEIOC-YTHDC2-only targets
MEIOC-only targets
E
MEIOC-YTHDC2-RBM46 targets
MEIOC-RBM46-only targets
MEIOC-YTHDC2-only targets
MEIOC-only targets
n=179
n=13
n=1135
n=284
n=184
n=12
n=1166
n=306
n=182
n=12
n=1108
n=259
n=181
n=11
n=1099
n=244
n=176
n=12
n=1011
n=199
F
MEIOC-YTHDC2-RBM46 targets
"Mitotic cell cycle" genes downregulated by MEIOC
171
16
277
Ccna2
Cdc25a
E2f6
Mcm6
Rad21
Ywhah
MEIOC-YTHDC2-RBM46 targets
"Meiotic cell cycle" genes upregulated by MEIOC
186
1
90
n.s.
Meioc

Figure 2: MEIOC-YTHDC2-RBM46 destabilize their mRNA targets.

A: Percentage of MEIOC targets within MEIOC-upregulated, MEIOC-downregulated, and expressed genes, defined by scRNA-seq. MEIOC targets were identified from reanalysis of a published RIP-seq dataset (Soh et al., 2017).

B: Cumulative fraction for $\log_2$ fold change (WT / *Meioc* KO), defined by scRNA-seq, with genes binned as MEIOC targets or nontargets.

C: Overlap of mRNAs identified by MEIOC RIP-seq, and YTHDC2 CLIP-seq, and RBM46 eCLIP-seq datasets. MEIOC RIP-seq data were reanalyzed from Soh et al., 2017. YTHDC2 CLIP-seq analysis was published in Saito et al., 2022. RBM46 eCLIP-seq data were reanalyzed from Qian et al., 2022. Asterisks denote statistical enrichment.

D: Percentage of MEIOC-YTHDC2-RBM46 targets, MEIOC-RBM46-only targets, MEIOC-YTHDC2-only targets, and MEIOC-only targets within MEIOC-downregulated and expressed genes.

E: Cumulative fraction for $\log_2$ fold change (WT / *Meioc* KO), defined by scRNA-seq, with genes binned as MEIOC-YTHDC2-RBM46 targets, MEIOC-RBM46-only targets, MEIOC-YTHDC2-only targets, and MEIOC-only targets. Asterisks represent comparison of color-matched target set to MEIOC-only targets.

F: MEIOC-YTHDC2-RBM46 targets are enriched for GO term “mitotic cell cycle” genes downregulated by MEIOC but not GO term “meiotic cell cycle” genes upregulated by MEIOC. Upregulated and downregulated genes were defined by scRNA-seq (any germ cell cluster). Asterisks represent statistical enrichment; “n.s.” represents “not significant” statistical enrichment or depletion.

*, adj. $P<0.05$; **, adj. $P<0.01$; ***, adj. $P<0.0001$; ****, adj. $P<0.0001$; n.s., not significant.

176 then compared how these groups respond to MEIOC in our scRNA-seq data. First, we examined
177 whether each of these groups was overrepresented among transcripts whose abundance
178 decreased in response to MEIOC. MEIOC-RBM46-YTHDC2 targets exhibited enrichment
179 beginning in mitotic spermatogonia (Fig. 2D). By contrast, MEIOC-RBM46-only targets were
180 enriched beginning at the transition from mitosis to meiosis, while MEIOC-only targets showed
181 no enrichment (Fig. 2D). Second, we examined the effect of YTHDC2 and RBM46 on the
182 stability of all MEIOC targets, irrespective of statistical cutoff. Relative to MEIOC-only targets,
183 MEIOC-RBM46-YTHDC2 targets exhibited the largest decrease in transcript abundance in all
184 scRNA-seq germ cell clusters (Fig. 2E), as well as in transcript stability in the bulk RNA-seq
185 analysis of preleptotene-enriched testes (Fig. S5B, S6B). Taken together, these data demonstrate
186 that MEIOC's destabilization of its target mRNAs occurs via its interaction with both YTHDC2
187 and RBM46.

188 Given that MEIOC-downregulated transcripts are enriched for "mitotic cell cycle"
189 factors, we hypothesized that MEIOC-YTHDC2-RBM46 is directly targeting and destabilizing
190 these factors. By comparing MEIOC-downregulated "mitotic cell cycle" transcripts to MEIOC-
191 YTHDC2-RBM46 targets, we discovered a small but statistically significant overlap that
192 included factors that impact cell cycle progression, such as *Ccna2* and *E2f6* (Fig. 2F). Some
193 targets were downregulated by MEIOC in mitotic spermatogonia and early during the mitosis-to-
194 meiosis transition, before "mitotic cell cycle" enrichment was evident among the MEIOC-
195 downregulated genes (Fig. 1C,D). Therefore, MEIOC's destabilization of mRNAs before and
196 during the mitosis-to-meiosis transition may impact spermatogenic cells' ability to establish a
197 meiosis-specific cell cycle program in meiotic prophase I spermatocytes.

198 We also considered the possibility that not all MEIOC-YTHDC2-RBM46 targets are
199 similarly regulated. In particular, given that MEIOC-upregulated transcripts are enriched for
200 "meiotic cell cycle" factors (Fig. 1C,D), we asked whether these transcripts were MEIOC-
201 YTHDC2-RBM46 targets. MEIOC-upregulated "meiosis cell cycle" transcripts and MEIOC-
202 YTHDC2-RBM46 targets shared one transcript, *Meioc* (Fig. 2F), with this overlap representing
203 neither statistical depletion nor enrichment. Therefore, MEIOC-YTHDC2-RBM46 does not
204 directly regulate the stability of meiosis-associated transcripts.
205 In total, MEIOC promotes the decay of its target transcripts beginning in mitotic
206 spermatogonia by acting with YTHDC2 and RBM46.
207
208 **MEIOC's destabilization of *E2f6* and *Mga* mRNA increases expression of E2F6- and MGA-**
209 **repressed genes**
210 The majority of MEIOC-regulated transcripts, as defined by RNA-seq analysis of wild-type
211 versus *Meioc*-null samples, do not directly interact with MEIOC-YTHDC2-RBM46 (Fig. 3A,
212 S6C). We examined whether these changes were dominated by altered transcript stabilities or
213 transcriptional rates. By applying REMBRANDTS to our bulk RNA-seq data, we estimated
214 change in mRNA abundance as change in exonic reads, change in pre-mRNA abundance (i.e.,
215 transcriptional rate) as change in intronic reads, and change in mRNA stability as the difference
216 between the change in exonic reads and that in intronic reads (Alkallas et al. 2017; Gaidatzis et
217 al. 2015). MEIOC-regulated transcripts exhibited large changes in transcriptional rates and
218 smaller changes in transcript stabilities (Fig. 3B). Therefore, MEIOC is mediating changes in
219 transcription, which then changes the abundance of transcripts not bound by MEIOC.

Figure 3

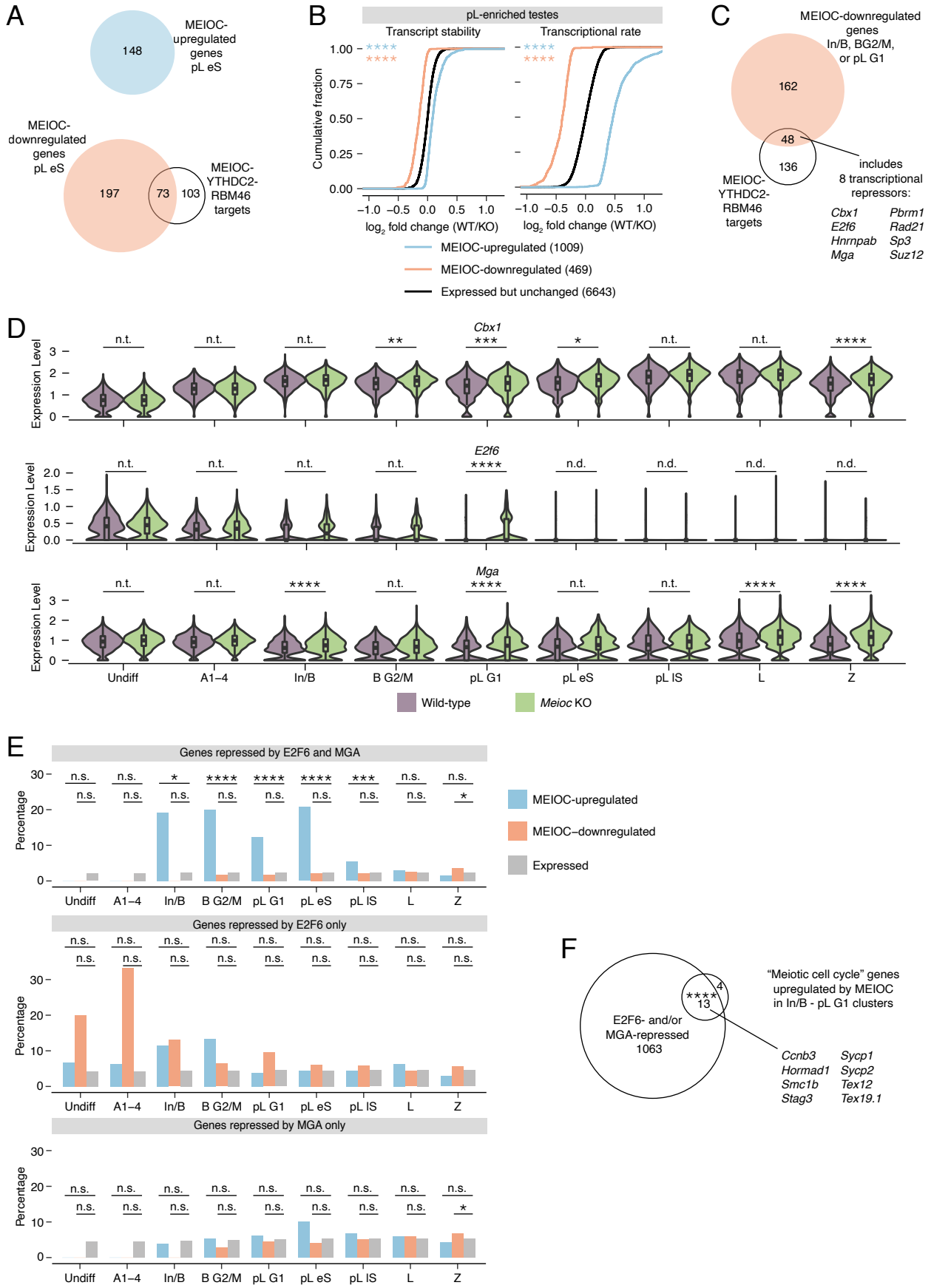
A
148
MEIOC-upregulated genes pL eS
MEIOC-downregulated genes pL eS
197
73
103
MEIOC-YTHDC2-RBM46 targets
B
pL-enriched testes
Transcript stability
Transcriptional rate
Cumulative fraction
log2 fold change (WT/KO)
MEIOC-upregulated (1009)
MEIOC-downregulated (469)
Expressed but unchanged (6643)
C
MEIOC-downregulated genes In/B, BG2/M, or pL G1
162
48
136
MEIOC-YTHDC2-RBM46 targets
includes 8 transcriptional repressors:
Cbx1 Pbrm1
E2f6 Rad21
Hnrnpab Sp3
Mga Suz12
D
Cbx1
E2f6
Mga
Expression Level
Undiff
A1–4
In/B
B G2/M
pL G1
pL eS
pL IS
L
Z
Wild-type
Meioc KO
E
Genes repressed by E2F6 and MGA
Genes repressed by E2F6 only
Genes repressed by MGA only
Percentage
MEIOC-upregulated
MEIOC–downregulated
Expressed
F
E2F6- and/or MGA-repressed 1063
4
13
"Meiotic cell cycle" genes upregulated by MEIOC in In/B - pL G1 clusters
Ccnb3 Sycp1
Hormad1 Sycp2
Smc1b Tex12
Stag3 Tex19.1

Figure 3: MEIOC-YTHDC2-RBM46's repression of *E2f6* and *Mga* mRNA relieves E2F6- and MGA-mediated transcriptional repression.

A: Venn diagram comparing MEIOC-upregulated and -downregulated genes in pL eS cluster to MEIOC-YTHDC2-RBM46 targets. The majority of genes whose transcript abundance changes in response to MEIOC are not directly targeted by MEIOC-YTHDC2-RBM46.

B: Cumulative distribution of $\log_2$ fold change (WT/ *Meioc* KO) for transcript stability (left) and transcriptional rate (right) for MEIOC-upregulated and MEIOC-downregulated genes compared to genes that expressed but do not change in response to MEIOC. Transcript stabilities and transcriptional rates were estimated using bulk RNA-seq data from preleptotene-enriched testes. Asterisks represent comparison of color-matched gene set to expressed but not regulated gene set.

C: Identification of MEIOC-YTHDC2-RBM46 targets that are downregulated by MEIOC in In/B, B G2/M, and/or pL G1 clusters. Of this set, 8 mRNAs encode proteins that have been reported to function as transcriptional repressors.

D: Expression levels for PRC1.6 subunits *Cbx1*, *E2f6*, and *Mga* in wildtype vs. *Meioc*-null cells in all germ cell clusters identified. *Cbx1*, *E2f6*, and *Mga* are downregulated by MEIOC in the In/B, B G2/M, and/or pL G1 clusters (adj. $P < 0.05$).

E: Percentage of genes repressed by E2F6 and MGA (top), E2F6 only (center), and MGA only (bottom) among MEIOC-upregulated, MEIOC-downregulated, and expressed genes. E2F6-repressed genes and MGA-repressed genes were identified via reanalysis of published ChIP-seq and RNA-seq datasets from mouse embryonic stem cells (Dahlet et al., 2021; Stielow et al., 2018; Zin et al., 2021).

F: Overlap between E2F6- and/or MGA-repressed genes and the "meiotic cell cycle" genes upregulated by MEIOC in In/B, B G2/M, and pL G1 clusters. Example genes that fall within this overlap are listed.

*, adj. $P<0.05$; **, adj. $P<0.01$; ***, adj. $P<0.001$; ****, adj. $P<0.0001$; n.s., not significant; n.t., not tested (comparison was excluded from statistical testing because $\log_2$ fold change> -0.1 and <0.1); n.d., not detected (transcript expressed in <25% cells in each population being compared).

220 Next, we sought to identify MEIOC targets that drive transcriptional changes. The vast
221 majority of MEIOC-upregulated transcripts are not directly bound by MEIOC (Fig. 2A, 3A). We
222 hypothesized that MEIOC-YTHDC2-RBM46 destabilizes a mRNA that encodes a
223 transcriptional repressor. Destabilization of this mRNA consequently derepresses (i.e.,
224 upregulates) gene expression. For this analysis, we focused on the In/B to pL G1 clusters, before
225 the spermatogenic cells have undergone the major MEIOC-dependent transcriptomic shift
226 observed in the scRNA-seq pseudotime analysis (Fig. 1A,B). Among the 48 MEIOC-YTHDC2-
227 RBM46 targets downregulated by MEIOC within the In/B to pL G1 clusters, we identified eight
228 mRNAs encoding transcriptional repressors: *Cbx1*, *E2f6*, *Hnrnpab*, *Mga*, *Pbrm1*, *Rad21*, *Sp3*,
229 and *Suz12* (Fig. 3C,D). Strikingly, *Cbx1*, *E2f6* and *Mga* all encode subunits of the noncanonical
230 Polycomb Repressive Complex (PRC) 1.6 (Fig. S7A, S9A), representing a statistically
231 significant enrichment for the complex's subunits (one-tailed hypergeometric test, P = 3.55E-
232 05). *E2f6* and *Mga* are particularly attractive candidates because they are sequence-specific
233 DNA-binding subunits of PRC1.6 required to repress meiosis-specific genes in somatic and
234 embryonic stem cells (Pohlers et al. 2005; Dahlet et al. 2021; Kehoe et al. 2008; Maeda et al.
235 2013; Suzuki et al. 2016; Kitamura et al. 2021; Uranishi et al. 2021).
236 We hypothesized that MEIOC-YTHDC2-RBM46's inhibition of *E2f6* and *Mga* was
237 impacting gene expression during spermatogenesis. To test this, we reanalyzed ChIP-seq and
238 RNA-seq datasets from mouse embryonic stem cells (Stielow et al. 2018; Qin et al. 2021; Dahlet
239 et al. 2021) to identify genes that are directly repressed by E2F6 or MGA (see Materials and
240 Methods; Fig. S8A,B). As E2F6 and MGA cooperate to repress expression of an overlapping set
241 of genes (Dahlet et al. 2021) (Fig. S8C), we classified genes as repressed by both E2F6 and
242 MGA, repressed by only E2F6, or repressed by only MGA. Genes repressed by both E2F6 and

243 MGA, but not those repressed by either protein alone, were overrepresented among MEIOC-
244 upregulated transcripts beginning in the mitotic In/B clusters, persisting through the mitosis-to-
245 meiosis transition (Fig. 3E). This enrichment was not seen in MEIOC-downregulated transcripts
246 (Fig. 3E). The bulk RNA-seq analysis of preleptotene-enriched testes largely confirmed these
247 results, while also revealing that MEIOC-upregulated genes were enriched for genes repressed
248 by only E2F6 and those repressed by only MGA (Fig. S9B), likely because this analysis included
249 lowly expressed genes that were not detected in the scRNA-seq analysis. Therefore, MEIOC's
250 repression of E2F6 and MGA upregulates gene expression as early as in mitotic spermatogonia.

251 We also examined whether MEIOC's repression of E2F6 and MGA leads to
252 downregulated gene expression in spermatogenic cells. For this analysis, we used the mouse
253 embryonic stem cell datasets to classify genes as activated by E2F6 and MGA, activated by only
254 E2F6, or activated by only MGA. Genes activated by only MGA showed modest enrichment in
255 MEIOC-downregulated genes within limited set of clusters (pL lS and L; Fig. S8D). Neither
256 MEIOC-upregulated nor -downregulated transcripts were enriched for genes activated by both
257 E2F6 and MGA or by only E2F6 (Fig. S8D). The bulk RNA-seq analysis of preleptotene-
258 enriched testes confirmed these results (Fig. S9B). Thus, MEIOC's repression of E2F6 and MGA
259 does not lead to broad downregulation of gene expression. Instead, MEIOC's repression of E2F6
260 and MGA primarily derepresses gene expression.

261 As many MEIOC-upregulated transcripts are meiotic cell cycle factors not bound by
262 MEIOC-YTHDC2-RBM46 (Fig. 1D, 2F), we hypothesized that repression of E2F6 and MGA
263 upregulates these meiotic genes. To test this, we asked whether E2F6- and MGA-repressed genes
264 are enriched among meiotic cell cycle transcripts upregulated by MEIOC. We again focused this
265 analysis on the In/B to pL G1 clusters, before germ cells have not undergone major MEIOC-

266 dependent transcriptomic changes. We found that 13 of 17 MEIOC-upregulated meiotic cell
267 cycle transcripts are targeted for repression by E2F6 and/or MGA (Fig. 3F). These observations
268 were also confirmed in the bulk RNA-seq analysis of preleptotene-enriched testes (Fig. S9C).
269 Therefore, MEIOC's destabilization of *E2f6* and *Mga* mRNAs de-represses meiosis-associated
270 gene expression beginning in mitotic spermatogonia.
271

272 **MEIOC indirectly activates transcriptional regulator STRA8-MEIOSIN to enhance**
273 **spermatogenic cells' competence to transition from mitosis to meiosis**

274 In mouse embryonic stem cells, E2F6 and MGA directly repress *Meiosin* (*Gm4969*) (Uranishi et
275 al. 2021) (Fig. S8A,B). Consistent with MEIOC's destabliization of *E2f6* and *Mga* mRNA, we
276 found that MEIOC upregulates *Meiosin* expression at both the transcript and protein levels
277 during the transition from mitosis to meiosis (Fig. 4A, S4C, S10A). By meiotic prophase I,
278 *Meioc*-null germ cells exhibited delayed upregulation of *Meiosin* expression (Fig. 4A). We
279 confirmed that *Meiosin* expression is also increased by YTHDC2 and RBM46, based on
280 previously reported analyses of bulk RNA-seq data from postnatal testes (Jain et al. 2018; Peart
281 et al. 2022). MEIOC does not bind *Meiosin* mRNA, nor does MEIOC affect other known
282 regulators of *Meiosin* gene expression (i.e., retinoic acid-dependent transcription and DMRT1
283 activity; Fig. S10, S11; see Supplemental Information) (Ishiguro et al. 2020). Based on these
284 data, MEIOC's repression of *E2f6* and *Mga* derepresses *Meiosin* gene expression during the
285 mitosis-to-meiosis transition.

286 STRA8-MEIOSIN functions as an obligate heterodimer that transcriptionally activates
287 gene expression during the transition from mitosis to meiosis (Ishiguro et al. 2020; Kojima et al.

Figure 4

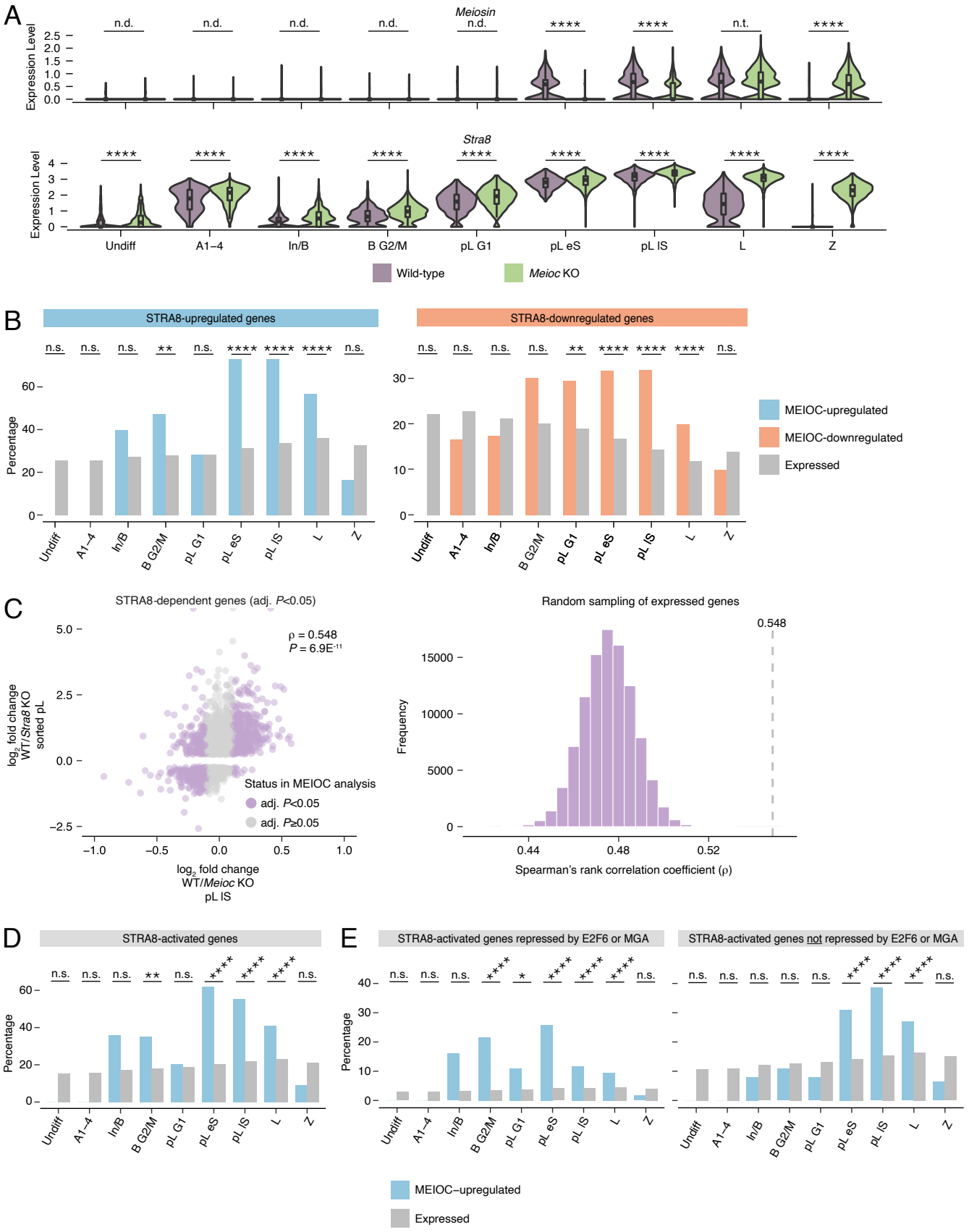
A
Meiosin
Stra8
Expression Level
n.d.
n.t.
****
Undiff
A1–4
In/B
B G2/M
pL G1
pL eS
pL lS
L
Z
Wild-type
Meioc KO
B
STRA8-upregulated genes
STRA8-downregulated genes
n.s.
**
****
Percentage
MEIOC-upregulated
MEIOC-downregulated
Expressed
C
STRA8-dependent genes (adj. P<0.05)
ρ = 0.548
P = 6.9E-11
log2 fold change WT/Stra8 KO sorted pL
log2 fold change WT/Meioc KO pL lS
Status in MEIOC analysis
adj. P<0.05
adj. P≥0.05
Random sampling of expressed genes
0.548
Frequency
Spearman's rank correlation coefficient (ρ)
D
STRA8-activated genes
E
STRA8-activated genes repressed by E2F6 or MGA
STRA8-activated genes not repressed by E2F6 or MGA
MEIOC–upregulated
Expressed

Figure 4: MEIOC's derepression of *Meiosin* gene expression enhances activation of the STRA8-MEIOSIN transcriptional program.

A: Expression levels of *Meiosin* and *Stra8* in wild-type and *Meioc* KO in all germ cell clusters. Clusters marked as "not done" (n.d.) did not meet expression thresholds set for statistical testing.

B: Percentage of STRA8-upregulated and -downregulated genes in MEIOC-upregulated, -downregulated, and expressed genes from scRNA-seq analysis. STRA8-upregulated and -downregulated genes were identified via reanalysis of bulk RNA-seq data from wild-type and *Stra8* KO sorted preleptotene spermatocytes from Kojima et al., 2019.

C: Left panel, correlation between MEIOC-dependent changes from scRNA-seq analysis of pL IS cluster and STRA8-dependent changes from bulk RNA-seq analysis of sorted preleptotene spermatocytes. Analysis was limited to genes that were statistically dependent on STRA8 (adjusted $P<0.05$). Right panel, distribution of correlations for gene sets obtained by random sampling of genes expressed in the scRNA-seq pL IS cluster and bulk RNA-seq sorted preleptotene spermatocytes.

D: Percentage of STRA8-activated genes in MEIOC-upregulated and expressed genes from scRNA-seq analysis. STRA8-activated genes were identified as those genes with STRA8-bound promoters (as identified by Kojima et al. (2019) via STRA8-FLAG ChIP-seq in preleptotene-enriched testes) and upregulated by STRA8 (as identified by reanalysis of bulk RNA-seq data from wild-type and *Stra8* KO sorted preleptotene spermatocytes from Kojima et al., 2019).

E: Percentage of STRA8-activated genes repressed by E2F6 or MGA (left), as well as STRA8-activated genes not repressed by E2F6 or MGA (right), in MEIOC-upregulated and expressed genes.

*, adj. $P<0.05$; **, adj. $P<0.01$; ***, adj. $P<0.001$; ****, adj. $P<0.0001$; n.s., not significant; n.t., not tested (comparison was excluded from statistical testing because $\log_2$ fold change> -0.1 and <0.1); n.d., not detected (transcript expressed in <25% cells in each population being compared).

288 2019). Here, we hypothesized that MEIOC's upregulation of *Meiosin* gene expression induces
289 STRA8-MEIOSIN-mediated transcriptional changes. We tested this hypothesis in three ways.
290 First, we asked if, during the mitosis-to-meiosis transition, MEIOC-dependent genes are
291 enriched for STRA8-dependent genes. We defined these STRA8-dependent genes by bulk RNA-
292 seq data from wild-type and *Stra8*-null preleptotene spermatocytes isolated via synchronization
293 and sorting (Kojima et al. 2019). We found that STRA8-upregulated genes were enriched among
294 MEIOC-upregulated genes during the mitosis-to-meiosis transition (pL eS and lS clusters) and in
295 meiotic prophase I (L cluster; Fig. 4B). Similarly, STRA8-downregulated transcripts were
296 enriched among MEIOC-downregulated transcripts at these same stages (Fig. 4B). The bulk
297 RNA-seq analysis of preleptotene-enriched testes revealed similar results (Fig. S12A).
298 Second, using STRA8-dependent genes, we correlated the transcript abundance changes
299 from the MEIOC scRNA-seq and STRA8 bulk RNA-seq datasets. STRA8-dependent genes
300 exhibited a statistically significant correlation between the MEIOC and STRA8 datasets that
301 peaked during the mitosis-to-meiosis transition (pL eS and lS clusters; Fig. 4C, S13A, S14A).
302 STRA8-dependent genes similarly exhibited a robust correlation between the MEIOC bulk
303 RNA-seq dataset from preleptotene-enriched testes and the STRA8 dataset (Fig. S12B).
304 Therefore, MEIOC supports STRA8-MEIOSIN-mediated changes in transcript abundance.
305 Third, we asked if MEIOC-dependent genes are enriched for genes directly activated by
306 STRA8-MEIOSIN. We defined STRA8-activated genes using ChIP-seq results from testes
307 enriched for preleptotene spermatocytes (Kojima et al. 2019) with the STRA8 bulk RNA-seq
308 analysis (see Materials and Methods). We found that MEIOC-upregulated genes were enriched
309 for STRA8-activated genes during the mitosis-to-meiosis transition (pL eS and lS clusters; Fig.
310 4D). This enrichment was also evident in the bulk RNA-seq analysis of preleptotene-enriched

311 testes (Fig. S12C). Furthermore, the top motif identified by de novo motif analysis of MEIOC-
312 upregulated genes from the bulk RNA-seq analysis matched the STRA8-MEIOSIN binding
313 motif (Fig. S12D). In total, ~60-70% of MEIOC-upregulated genes are directly activated by
314 STRA8-MEIOSIN.

315 Together, these analyses demonstrate that MEIOC indirectly activates the STRA8-
316 MEIOSIN transcriptional regulator during the transition from mitosis to meiosis, facilitating a
317 major transcriptomic shift at the meiotic G1/S transition (Fig. 1A). With this new molecular
318 insight, we revisited our interpretation of the *Meioc*-null phenotype. Based on prior histological
319 analysis, *Meioc*-null spermatogenic cells accumulate at the preleptotene stage and are delayed in
320 entering the leptotene stage (Soh et al. 2017; Abby et al. 2016). This is phenotypically distinct
321 from spermatogenic cells that lack the developmental competence to transition from mitosis to
322 meiosis, as *Stra8*-null or *Meiosin*-null cells on the same genetic background arrest at the
323 preleptotene stage (Ishiguro et al. 2020; Kojima et al. 2019; Anderson et al. 2008b). Given that
324 *Meioc*-null germ cells still exhibit some *Meiosin* expression, we interpret the *Meioc*-null
325 phenotype as delayed acquisition of the developmental competence to transition from mitosis to
326 meiosis. Therefore, MEIOC enhances spermatogenic cells' competence to initiate meiosis by
327 activating the STRA8-MEIOSIN transcriptional regulator.

328

329 **MEIOC derepresses meiotic gene expression before activating STRA8-MEIOSIN**

330 We observed that many STRA8-activated genes are also repressed by E2F6 and/or MGA (Fig.
331 S12E). As MEIOC represses E2F6 and MGA in mitotic spermatogonia and activates STRA8-
332 MEIOSIN during the mitosis-to-meiosis transition, we hypothesized that MEIOC-regulated
333 genes exhibit temporally distinct regulation, dependent on whether they were targeted by only

334 STRA8-MEIOSIN or by both E2F6-MGA and STRA8-MEIOSIN. Specifically, we predicted
335 that genes experimentally defined as E2F6 and/or MGA-repressed and STRA8-activated would
336 be upregulated by MEIOC starting in mitotic spermatogonia, coincident with MEIOC's
337 destabilization of *E2f6* and *Mga*. By contrast, STRA8-activated genes that were not repressed by
338 E2F6 or MGA would only be upregulated by MEIOC later during the mitosis-to-meiosis
339 transition, coincident with MEIOC's upregulation of *Meiosin* gene expression. Indeed, consistent
340 with our predictions, STRA8-activated, E2F6-MGA-repressed genes were enriched among
341 MEIOC-upregulated genes in the mitotic B G2/M cluster as well as during the mitosis-to-meiosis
342 transition (pL G1, eS, and lS clusters; Fig. 4E). By contrast, STRA8-activated genes that were
343 not repressed by E2F6 or MGA exhibited enrichment during the pL eS and lS clusters (Fig. 4E).
344 Both gene sets were also enriched among MEIOC-upregulated genes in the bulk RNA-seq
345 analysis (Fig. S12F). Therefore, during late transit amplification, MEIOC derepresses a set of
346 meiotic genes targeted by E2F6 and MGA; then during the mitosis-to-meiosis transition, MEIOC
347 increases the expression of these and other meiotic genes by activating STRA8-MEIOSIN.
348 In total, MEIOC-YTHDC2-RBM46's destabilization of *E2f6* and *Mga* mRNAs in late
349 mitotic spermatogenic cells derepresses E2F6-MGA-targeted genes, including *Meiosin* and other
350 meiosis-associated genes. In turn, this activity supports activation of the STRA8-MEIOSIN
351 transcriptional regulator by retinoic acid during the transition from mitosis to meiosis (Fig. 5). As
352 STRA8-MEIOSIN is the molecular vehicle by which retinoic acid induces the meiotic G1/S
353 transition, MEIOC's regulation of the STRA8-MEIOSIN complex enhances spermatogenic cells'
354 competence to undergo the mitosis-to-meiosis transition.

Figure 5

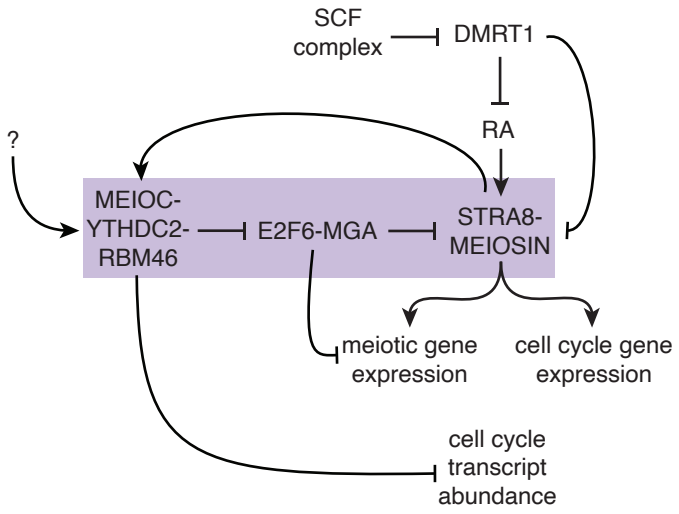

Figure 5: Model for MEIOC-YTHDC2-RBM46 enhancing spermatogenic cells' competence to transition from mitosis to meiosis in response to retinoic acid.

MEIOC-YTHDC2-RBM46 destabilize *E2f6* and *Mga* mRNA and thereby inhibit E2F6 and MGA's repression of transcription at genes involved in meiosis, including *Meiosin*. In parallel, the SCF complex degrades DMRT1 and consequently inhibits DMRT1's repression of retinoic acid (RA)-dependent transcription as well as *Stra8* and *Meiosin* gene expression. Retinoic acid activates *Stra8* and *Meiosin* gene expression. This activates the STRA8-MEIOSIN transcription factor, which drives the transcription of cell cycle genes as well as meiotic genes, many of which were previously repressed by E2F6 and MGA. MEIOC's repression of cell cycle transcripts also contributes to the establishment of a meiosis-specific cell cycle program in meiotic prophase I. The question mark denotes undefined molecular regulation that activates MEIOC-YTHDC2-RBM46 before retinoic acid activates STRA8-MEIOSIN transcriptional activity and the transition from mitosis to meiosis. Box highlights the novel regulation identified in this study that facilitates competence for the mitosis-to-meiosis transition.

355 **DISCUSSION**

356 Here we use scRNA-seq, as well as bulk RNA-seq of developmentally synchronized and
357 histologically staged spermatogenesis, to demonstrate that *Meioc*-null spermatogenic cells
358 developmentally diverge from their wild-type counterparts during the meiotic G1/S transition,
359 earlier than previously appreciated. We find that MEIOC is required to derepress expression of
360 meiotic genes, including the meiotic transcriptional regulator *Meiosin*. In turn, MEIOC increases
361 the expression of genes targeted by STRA8-MEIOSIN, which drives the mitosis-to-meiosis
362 transition. Therefore, MEIOC enhances differentiating spermatogonia's competence to activate
363 the meiotic transcriptional regulator and transition from mitosis to meiosis in response to retinoic
364 acid.

365 We find that MEIOC-YTHDC2-RBM46 destabilizes its mRNA targets, as has been
366 suggested previously based on analyses of transcript abundance (Saito et al. 2022; Hsu et al.
367 2017; Soh et al. 2017; Qian et al. 2022). In the current study, we distinguished changes in
368 transcription vs. transcript stability via two approaches. First, scRNA-seq allowed us to identify
369 and analyze spermatogenic cells that had been impacted by MEIOC before the onset of major
370 transcriptional changes. Second, we applied a specialized pipeline to distinguish between
371 transcriptional rate and RNA stability in bulk RNA-seq data of preleptotene-enriched testes
372 (Alkallas et al. 2017). Both complementary methods confirm that MEIOC-YTHDC2-RBM46
373 reduces the stability of its target transcripts. Transcript stability may be the primary mechanism
374 by which MEIOC-YTHDC2-RBM46 regulates its targets, as a recent study found that YTHDC2
375 does not affect translation in postnatal testes (Saito et al. 2022). Whether MEIOC-YTHDC2-
376 RBM46 impacts transcript localization remains to be examined.

377 Beginning in mitotic spermatogonia, MEIOC-YTHDC2-RBM46 increases the abundance
378 of meiosis-associated transcripts without directly binding many of these transcripts. Here, we
379 demonstrate that these transcript abundance changes are driven by changes in transcription rather
380 than mRNA stability (Fig. 3B). Further, we provide a two-tiered mechanism for these indirect
381 changes in transcript abundance. First, MEIOC-YTHDC2-RBM46 binds to and destabilizes *E2f6*
382 and *Mga* mRNAs, which encode transcriptional repressors whose genomic targets are enriched
383 for meiosis-associated genes (Pohlers et al. 2005; Dahlet et al. 2021; Kehoe et al. 2008; Maeda et
384 al. 2013; Suzuki et al. 2016; Kitamura et al. 2021; Uranishi et al. 2021). Second, MEIOC-
385 YTHDC2-RBM46's repression of *E2f6* and *Mga* derepresses *Meiosin* gene expression and
386 activates STRA8-MEIOSIN. This transcriptional regulator then activates meiotic gene
387 expression and the meiotic G1/S transition. Thus, MEIOC-YTHDC2-RBM46's repression of a
388 transcriptional repressor confers developmental competence to transition from mitosis to
389 meiosis.

390 In embryonic oocytes, loss of PRC1 activity via genetic ablation of *Ring1* and *Rnf2*
391 causes premature meiosis due to precocious expression of *Stra8* and other meiosis-associated
392 genes (Yokobayashi et al. 2013). Therefore, it is plausible that, during spermatogenesis, PRC1
393 also regulates gene expression and the timing of meiotic initiation, but this has not been directly
394 tested. In addition, the germline activity of PRC1.6 subunits E2F6 and MGA remains poorly
395 characterized. While *E2f6*-null mice are fertile, spermatogenesis was reported as disrupted
396 without detailed characterization (Storre et al. 2002). Genetic ablation of *Mga* causes embryonic
397 lethality, precluding any analysis of spermatogenesis (Burn et al. 2018; Washkowitz et al. 2015).
398 Therefore, additional genetic studies are needed to identify E2F6 and MGA's function during
399 spermatogenesis and to determine the extent to which loss of *E2f6* and *Mga* can rescue the

400 developmental competence of *Meioc*-null spermatogenic cells. In addition, it is possible that
401 other transcriptional repressors targeted by MEIOC-YTHDC2-RBM46 may also control *Meiosin*
402 gene expression.

403 As some *Meioc*-null spermatogenic cells upregulate *Meiosin* gene expression and enter
404 meiotic prophase I along a delayed timeline, MEIOC is not strictly required for the competence
405 to transition from mitosis to meiosis. It is possible that residual activity from YTHDC2-RBM46
406 in the absence of MEIOC can support meiotic entry in some cells; alternatively, the DMRT1-
407 mediated acquisition of competence may support mitotic spermatogonia's competence to
408 transition from mitosis to meiosis along this delayed timeline. Regardless, our model establishes
409 that the *Meioc*, *Ythdc2*, and *Rbm46*-null phenotype of delayed entry into meiotic prophase I is the
410 result of reduced STRA8-MEIOSIN transcriptional activation and is therefore the less severe
411 manifestation of the arrest at the mitotic-to-meiosis transition, before meiotic prophase I,
412 exhibited by *Stra8* and *Meiosin*-null spermatogenic cells on an inbred C57BL/6 background.
413 Intriguingly, *Stra8*-null spermatogenic cells on a mixed genetic background exhibit the less
414 severe phenotype similar to *Meioc*, *Ythdc2*, and *Rbm46*-null spermatogenic cells. Our analyses of
415 the *Meioc*-null phenotype suggest that on a mixed genetic background, the *Stra8*-null
416 spermatogenic cells contain residual transcriptional activation of some meiotic gene expression,
417 potentially due to MEIOSIN acting as a homodimer, but further work is needed to test this
418 prediction.

419 Our model for mammalian meiotic initiation exhibits parallels, without direct orthology
420 or homology, to the molecular network that governs budding yeast meiotic initiation.
421 Specifically, repression of a transcriptional repressor (Rme1p) via mRNA destabilization
422 activates expression of the key transcription factor (Ime1p) that governs meiotic entry.

423 Therefore, in both unicellular eukaryotes and multicellular organisms, destabilization of a
424 transcriptional repressor at the transcript level controls activation of the meiotic transcriptional
425 program.

426 We have placed transcriptional activation by STRA8-MEIOSIN and post-transcriptional
427 repression of mRNA by MEIOC-YTHDC2-RBM46 in a positive feedback loop that facilitates
428 the mitosis-to-meiosis transition (Fig. 5). This model also generates a new question: how is
429 MEIOC-YTHDC2-RBM46 activated before retinoic acid activates STRA8-MEIOSIN and the
430 transition from mitosis to meiosis (Fig. 5)? One possibility is illustrated by MEIOC and
431 YTHDC2's *Drosophila* homologs Bam and Bgcn, which (translationally) repress their mRNA
432 targets in late mitotic spermatogonia to facilitate the transition from mitosis to meiosis (Insco et
433 al. 2009, 2012). This transition requires the accumulation of Bam protein to a critical threshold
434 (Insco et al. 2009). Whether mammalian MEIOC must similarly accumulate to a critical
435 threshold to activate the MEIOC-YTHDC2-RBM46 complex requires further investigation.

436 In conclusion, by functioning as a destabilizer of its mRNA targets, MEIOC-YTHDC2-
437 RBM46 represses transcriptional repressors E2F6 and MGA and thereby allows spermatogenic
438 cells to activate *Meiosin* expression in response to retinoic acid. Consequently, this activates the
439 key meiotic transcriptional regulator STRA8-MEIOSIN, which amplifies expression of meiosis-
440 and cell cycle-associated genes and drives the meiotic G1/S transition. In total, the post-
441 transcriptional activity of MEIOC-YTHDC2-RBM46 enhances the activity of the meiotic
442 transcriptional regulator. This regulation, acting as a second, parallel mechanism to the SCF
443 complex's degradation of DMRT1, enhances mitotic spermatogonia's competence to transition
444 from mitosis to meiosis in response to retinoic acid.

445 **MATERIALS AND METHODS**

446 *Animals*

447 All experiments involving mice were performed in accordance with the guidelines of the
448 Massachusetts Institute of Technology (MIT) Division of Comparative Medicine and Cincinnati
449 Children's Hospital Medical Center (CCHMC) Division of Veterinary Services, which are
450 overseen by their respective Institutional Animal Care and Use Committees (IACUC). The
451 animal care programs at MIT/Whitehead Institute and CCHMC are accredited by the Association
452 for Assessment and Accreditation of Laboratory Animal Care, International (AAALAC) and
453 meet or exceed the standards of AAALAC as detailed in the Guide for the Care and Use of
454 Laboratory Animals. This research was approved by the MIT IACUC (no. 0617-059-20) and
455 CCHMC IACUC (no. 2022-0061).

456 Mice carrying the *Meioc*-null allele *Meioc*$^{tm1.1Dpc}$ (Soh et al. 2017) were backcrossed to
457 C57BL/6N (B6N) from Taconic Biosciences for at least 10 generations. Mice used for scRNA-
458 seq experiments were also heterozygous for *Hspa2*^{tm1Dix} (RRID: IMSR_JAX:013584;(Dix et al.
459 1996)) and homozygous for *Gt(ROSA)26Sor*$^{tm9(CAG\text{-}tdTomato)Hze}$ (*ROSA26*^{tdTomato};
460 RRID:IMSR_JAX:007909; (Madisen et al. 2010)) with the floxed stop codon intact; both of
461 these genotypes exhibit normal spermatogenesis.

462

463 *10x Genomics single-cell RNA-seq*

464 Single-cell sequencing libraries were prepared and sequenced in two batches, with each batch
465 containing one wild-type and one *Meioc*-null pup at P15. One P15 testis per pup was
466 enzymatically dissociated into single cells (see Supplemental Information) and resuspended in
467 0.05% bovine serum albumin (BSA) in phosphate buffered saline (PBS) for a target

468 concentration of 1000 cells per microliter. Cell suspensions were loaded onto the Chromium
469 Controller, aiming for recovery of 10,000 cells per sample. Libraries were generated using the
470 Chromium Next GEM Single Cell 3′ v3.1 (10x Genomics), according to manufacturer's
471 instructions, and sequenced as 150 bp paired-end reads on an Illumina NovaSeq 6000 system
472 with an S4 flow cell.
473
474 *Analysis of 10x Genomics scRNA-seq data*
475 Alignment, filtering, barcode counting, and UMI counting were done via *count* function in Cell
476 Ranger v.4.0.0 with default settings using Cell Ranger's mm10-2020-A reference package (i.e.,
477 the GRCm38/mm10 mouse genome assembly with GENCODE vM23/Ensembl 98 annotation).
478 Using Seurat v.3.2.3 (Stuart et al. 2019), cells were filtered for less than 10% mitochondrial
479 reads, more than 1000 detected features, and a doublet score (generated by the *bcds* in scds
480 v.1.2.0) of less than 0.4. Using protein-coding genes, UMI counts from both wild-type and
481 *Meioc*-null samples were integrated and clusters identified using the first 30 dimensions. The
482 wild-type samples were used to assign cell types to clusters, first using cell type-enriched gene
483 expression (Fig. S1B) and refined based on cell cycle phase using the *CellCycleScoring* function
484 in Seurat (Fig. S1C,D). Clusters were merged as needed, and clusters with less than five cells
485 were removed. Cell cycle designations of the preleptotene clusters were confirmed via gene
486 expression patterns in wild-type cells independent of the gene:cell cycle phase pairings used by
487 Seurat's *CellCycleScoring* function (see Supplemental Information). These final cell type
488 designations were then applied to the *Meioc*-null samples. An additional spermatocyte cluster
489 (labeled Mut) was identified in the *Meioc*-null samples that was not identified in the wild-type
490 samples. In addition to the germ cell and somatic clusters shown in Fig. S1A,B, one additional

491 somatic cluster and one additional germ cell cluster were also identified but could not be
492 assigned a cell type using marker expression. These unassigned somatic and germ cell clusters,
493 along with all other somatic clusters, were excluded from subsequent analyses. See Supplemental
494 Information for additional details on cluster-specific enrichment or depletion in wild-type cells
495 and Gene Set Enrichment Analysis (GSEA).

496 The pseudotime trajectory was built in Monocle 3 v1.0.0 (Trapnell et al. 2014; Qiu et al.
497 2017a, 2017b) using the following procedure: the Seurat object containing germ cell clusters
498 only was imported as a Monocle object; data were normalized and pre-processed (function
499 *preprocess_cds()*; options: num_dim = 100); batch effects were removed (function *align_cds()*;
500 options: alignment_group = "batch"), dimensionality reduction was done via UMAP (function
501 *reduce_dimension()*); cells were clustered (function *cluster_cells()*); a principal graph was
502 learned from the reduced dimension space (function *learn_graph()*); and cells were ordered by
503 selecting the Undiff cluster as the starting branch of the trajectory (function *order_cells()*).
504 Cluster cell-type assignments made in Seurat were maintained in the pseudotime trajectory.

505 For differential expression analysis between wild-type and *Meioc*-null germ cells $\log_2$
506 fold change was defined as wild-type over *Meioc*-null germ cells, such that the value reflects
507 MEIOC's activity in the unperturbed wild-type state. Differential expression analysis of scRNA-
508 seq data was done on each germ cell cluster on genes with a minimum absolute $\log_2$ fold change
509 of 0.1 and that were detected in at least 25% of either population using Seurat's *FindMarkers*
510 function (options: logfc.threshold = 0.1, min.pct = 0.25); *P* values were adjusted for multiple
511 hypothesis testing of tested genes across all 9 germ cell clusters via the Bonferroni correction
512 using the *p.adjust* function in R. Additional expressed genes (i.e., detected in at least 25% of
513 cells in wild-type or *Meioc*-null cells per cluster) that failed to meet the $\log_2$ fold change

514 threshold for differential expression testing were identified via the *FindMarkers* function
515 (options: logfc.threshold=0, min.pct = 0.25), and their *P* values were marked as "nd" for
516 differential expression testing "not done."
517 Dot plots were generated using Seurat's *DotPlot* function with parameter scale=FALSE
518 to maintain average expression from wild-type and *Meioc*-null samples on the same scale.
519
520 *Synchronization of spermatogenesis*
521 Spermatogenesis was synchronized using a protocol originally developed by Hogarth et al.
522 (Hogarth et al. 2013) and modified by Romer et al. (Romer et al. 2018).
523
524 *Bulk RNA-seq analysis of preleptotene-enriched testes*
525 Total RNA was extracted from 4 wild-type samples and 3 *Meioc*-null samples, using 1.5
526 synchronized testes from a single pup per sample. TRIzol Reagent (Thermo Fisher Scientific)
527 was added to freshly thawed whole testes, and ERCC RNA ExFold RNA Spike-In Mix 1 and 2
528 (Thermo Fisher Scientific) were added to wild-type and *Meioc*-null samples, respectively, at a
529 concentration of 1 μl of a 1:100 dilution of spike-in mix per 1 mg of testis tissue. (Spike-in mixes
530 were ultimately not used for data analysis.) Total RNA was then isolated with chloroform
531 following the manufacturer's protocol, precipitated via isopropanol, and resuspended in RNase-
532 free water. RNA-seq libraries were prepared with the TruSeq Stranded Total RNA kit with the
533 Ribo-Zero Gold rRNA Removal kit. The barcoded libraries were pooled and sequenced with
534 50bp single-end reads on an Illumina HiSeq 2500 machine.
535 Reads were quality trimmed using cutadapt v1.8 (options: -q 30 --minimum-length 20 -b
536 AGATCGGAAGAGC). Expression levels of all transcripts in the mouse Gencode Basic vM15

537 gene annotation were estimated using kallisto v0.44.0 (Bray et al. 2016) with sequence-bias
538 correction (--bias) and strand-specific pseudoalignment (--rf-stranded). Quantified transcripts
539 were filtered for protein-coding genes, transcript-level estimated counts and transcripts per
540 million (TPM) values were summed to the gene level, and TPMs were renormalized to
541 transcript-per-million units.

542 To identify the MEIOC-dependent differential expression program, read counts from
543 kallisto were rounded to the nearest integer and then supplied to DESeq2 v1.26.0 (Love et al.
544 2014). Genes were filtered for a minimum TPM of 1 in at least 3 of 7 2S preleptotene samples,
545 and differential expression/abundance was defined using a cutoff of adjusted P value < 0.05.

546 For analysis of transcript stability and transcriptional rates, reads were mapped to the
547 mouse genome (mm10) with the GENCODE Basic vM15 gene annotation via STAR v2.7.1a
548 (Dobin et al. 2013) (options: --outFilterMultimapNmax 1 --alignEndsType Extend5pOfRead1 --
549 outFilterMismatchNmax 2 --outSAMattributes None). All other parameters were set to default.
550 Counts were quantified by htseq v0.11.0 (options: -m union --stranded=reverse) at the gene level
551 (-type gene) and exon level (-type exon), and intron levels were calculated as gene-level counts
552 minus exon-level counts. Changes in transcript stability, transcriptional rate, and abundance were
553 calculated for each gene for each sample using REMBRANDTS (Alkallas et al. 2017) with a
554 stringency of 0.80 and linear bias mode. The change between wild-type and *Meioc*-null samples
555 was then calculated in R.

556

557 *Re-analysis of STRA8 RNA-seq dataset*

558 RNA-seq data from *Stra8*-null and *Stra8*-heterozygote (i.e., phenotypically wild-type)
559 preleptotene spermatocytes (NCBI GEO GSE115928; Kojima et al. 2019) were reanalyzed.

560 Genes with STRA8-bound promoters identified by ChIP-seq in testes enriched for preleptotene
561 spermatocytes were extracted from Supplementary File 2 (Kojima et al. 2019)
562 (https://doi.org/10.7554/eLife.43738.028). See Supplemental Information for details.
563
564 *Gene Ontology analysis of scRNA-seq and bulk RNA-seq data*
565 Within each scRNA-seq cluster, MEIOC-upregulated ($\log_2$ fold change > 0.1 and adjusted *P*
566 value < 0.05) and MEIOC-downregulated genes ($\log_2$ fold change < -0.1 and adjusted *P* value <
567 0.05) were separately tested for enrichment of Gene Ontology Biological Processes gene lists
568 relative to a background of all expressed genes (i.e., genes expressed in at least 25% of wild-type
569 or *Meioc*-null cells within that cluster). For bulk RNA-seq data, MEIOC-upregulated ($\log_2$ fold
570 change > 0 and adjusted *P* value < 0.05) and MEIOC-downregulated genes ($\log_2$ fold change < -
571 0.1 and adjusted *P* value < 0.05) were similarly tested against a background of all expressed
572 genes (i.e., a minimum TPM of 1 in at least 3 of 7 2S preleptotene samples). These analyses were
573 done via R package clusterProfiler v3.0.4 using the *enrichGO* function (options: OrgDb =
574 "org.Mm.eg.db", ont = "BP", pvalueCutoff = 0.05, readable = T, pAdjustMethod = "BH"). For
575 the scRNA-seq data, the average $\log_2$ fold change for select upregulated and downregulated
576 genes that fell under GO terms “meiotic cell cycle” (GO:0051321) and “mitotic cell cycle”
577 (GO:0000278), respectively, were graphed via heatmap to show gene expression changes
578 between wild-type and *Meioc*-null cells across scRNA-seq germ cell clusters.
579
580 *Re-analysis of MEIOC RIP-seq dataset and comparison to YTHDC2 and RBM46 CLIP datasets*
581 MEIOC RIP-seq from P15 testes (NCBI GEO GSE96920; Soh et al. 2017) were reanalyzed, with
582 additional details in Supplemental information.

583 YTHDC2-bound mRNAs identified via CLIP-seq in P8 and P10 testes were extracted
584 from Tables S1 and S2 (Saito et al. 2022)
585 (http://genesdev.cshlp.org/content/suppl/2022/01/19/gad.349190.121.DC1/Supplemental_Tables.
586 xlsx).
587 RBM46 eCLIP data from P12-P14 testes (NCBI GEO GSE197282) (Qian et al. 2022)
588 were reanalyzed, with additional details in Supplemental Information.
589
590 *Re-analysis of E2F6 and MGA ChIP-seq datasets and RNA-seq datasets from ESCs*
591 The following datasets were reanalyzed here: E2F6 ChIP-seq and input data from wild-type and
592 *E2f6*-knockout mouse ESCs (NCBI GEO GSE149025) (Dahlet et al. 2021); MGA and IgG
593 ChIP-seq from wild-type mouse ESCs (ArrayExpress E-MTAB-6007) (Stielow et al. 2018);
594 mouse ESC RNA-seq data from wild-type and *E2f6*-knockout samples (NCBI GEO
595 GSE149025) (Dahlet et al. 2021); and wild-type and *Mga*-knockout samples (NCBI GEO
596 GSE144141) (Qin et al. 2021). See Supplemental Information for details.
597

598 **Competing Interest Statement**

599 The authors declare no competing interests.

600

601 **Acknowledgements**

602 We thank Kei-Ichiro Ishiguro for the MEIOSIN antibody; Mary Goodheart, Mina Kojima, Holly
603 Christensen, and Peter Nicholls for technical help; and Abigail Groff and Linyong Mao for
604 advice on bioinformatics analysis. We are grateful to the members of the Page Lab for valuable
605 feedback, and to Winston Bellott, Jordana Bloom, ZY Chen, Jennifer Hughes, Mina Kojima, and
606 Adrianna San Roman for comments on the manuscript.

607 We thank the Whitehead Genome Technology Core for library preparation and Illumina
608 sequencing, and the Whitehead Institute FACS Facility for cell sorting. Fluorescent microscopy
609 was done at the WM Keck Foundation Biological Imaging Facility at the Whitehead Institute and
610 Cincinnati Children's Bio-Imaging and Analysis Facility (RRID:SCR_022628).

611 This work was supported by Eunice Kennedy Shriver National Institute of Child Health
612 and Human Development of the National Institutes of Health under Award Numbers
613 F32HD093391 (M.M.M), K99HD097285 (M.M.M), and R00HD097285 (M.M.M) as well as the
614 Howard Hughes Medical Institute, where D.C.P. is an Investigator.

615

616 **Author Contributions**

617 M.M.M and B.L. prepared samples for 10x Genomic analysis. D.deR. assessed germ cell stage in
618 synchronized testis samples. M.M.M. performed all other experiments and data analysis.
619 M.M.M. and D.C.P. designed the study and wrote the manuscript with contributions from all
620 authors.

621 **REFERENCES**

622 Abby E, Tourpin S, Ribeiro J, Daniel K, Messiaen S, Moison D, Guerquin J, Gaillard J-C,
623 Armengaud J, Langa F, et al. 2016. Implementation of meiosis prophase I programme
624 requires a conserved retinoid-independent stabilizer of meiotic transcripts. *Nat Commun*
625 **7**: 10324.

626 Alkallas R, Fish L, Goodarzi H, Najafabadi HS. 2017. Inference of RNA decay rate from
627 transcriptional profiling highlights the regulatory programs of Alzheimer's disease. *Nat*
628 *Commun* **8**: 909.

629 Anderson EL, Baltus AE, Roepers-Gajadien HL, Hassold TJ, de Rooij DG, van Pelt AMM, Page
630 DC. 2008a. Stra8 and its inducer, retinoic acid, regulate meiotic initiation in both
631 spermatogenesis and oogenesis in mice. *Proc Natl Acad Sci U S A* **105**: 14976–14980.

632 Anderson EL, Baltus AE, Roepers-Gajadien HL, Hassold TJ, de Rooij DG, van Pelt AMM, Page
633 DC. 2008b. Stra8 and its inducer, retinoic acid, regulate meiotic initiation in both
634 spermatogenesis and oogenesis in mice. *Proc Natl Acad Sci U S A* **105**: 14976–14980.

635 Bailey AS, Batista PJ, Gold RS, Chen YG, de Rooij DG, Chang HY, Fuller MT. 2017. The
636 conserved RNA helicase YTHDC2 regulates the transition from proliferation to
637 differentiation in the germline. *eLife* **6**.

638 Baltus AE, Menke DB, Hu Y-C, Goodheart ML, Carpenter AE, de Rooij DG, Page DC. 2006. In
639 germ cells of mouse embryonic ovaries, the decision to enter meiosis precedes premeiotic
640 DNA replication. *Nat Genet* **38**: 1430–1434.

641 Bray NL, Pimentel H, Melsted P, Pachter L. 2016. Near-optimal probabilistic RNA-seq
642 quantification. *Nat Biotechnol* **34**: 525–527.

643 Burn SF, Washkowitz AJ, Gavrilov S, Papaioannou VE. 2018. Postimplantation Mga expression
644 and embryonic lethality of two gene-trap alleles. *Gene Expr Patterns GEP* **27**: 31–35.

645 Chen D, Wu C, Zhao S, Geng Q, Gao Y, Li X, Zhang Y, Wang Z. 2014. Three RNA binding
646 proteins form a complex to promote differentiation of germline stem cell lineage in
647 Drosophila ed. M.T. Fuller. *PLoS Genet* **10**: e1004797.

648 Dahlet T, Truss M, Frede U, Al Adhami H, Bardet AF, Dumas M, Vallet J, Chicher J, Hammann
649 P, Kottnik S, et al. 2021. E2F6 initiates stable epigenetic silencing of germline genes
650 during embryonic development. *Nat Commun* **12**: 3582.

651 Dix DJ, Allen JW, Collins BW, Mori C, Nakamura N, Poorman-Allen P, Goulding EH, Eddy
652 EM. 1996. Targeted gene disruption of Hsp70-2 results in failed meiosis, germ cell
653 apoptosis, and male infertility. *Proc Natl Acad Sci U S A* **93**: 3264–3268.

654 Dobin A, Davis CA, Schlesinger F, Drenkow J, Zaleski C, Jha S, Batut P, Chaisson M, Gingeras
655 TR. 2013. STAR: Ultrafast universal RNA-seq aligner. *Bioinformatics* **29**: 15–21.

656 Dokshin GA, Baltus AE, Eppig JJ, Page DC. 2013. Oocyte differentiation is genetically
657 dissociable from meiosis in mice. *Nat Genet* **45**: 877–883.

658 Endo T, Romer KA, Anderson EL, Baltus AE, de Rooij DG, Page DC. 2015. Periodic retinoic
659 acid-STRA8 signaling intersects with periodic germ-cell competencies to regulate
660 spermatogenesis. *Proc Natl Acad Sci U S A* **112**: E2347-56.

661 Gaidatzis D, Burger L, Stadler MB. 2015. Analysis of intronic and exonic reads in RNA-seq data
662 characterizes transcriptional and post-transcriptional regulation. *Nat Biotechnol* **33**: 722–
663 9.

664 Gonczy P, Matunis E, DiNardo S. 1997. bag-of-marbles and benign gonial cell neoplasm act in
665 the germline to restrict proliferation during Drosophila spermatogenesis. *Development*
666 **124**: 4361–4371.

667 Hogarth CA, Evanoff R, Mitchell D, Kent T, Small C, Amory JK, Griswold MD. 2013. Turning
668 a spermatogenic wave into a tsunami: synchronizing murine spermatogenesis using WIN
669 18,446. *Biol Reprod* **88**: 1–9.

670 Hsiao CJ, Tung P, Blischak JD, Burnett JE, Barr KA, Dey KK, Stephens M, Gilad Y. 2020.
671 Characterizing and inferring quantitative cell cycle phase in single-cell RNA-seq data
672 analysis. *Genome Res* **30**: 611–621.

673 Hsu PJ, Zhu Y, Ma H, Guo Y, Shi X, Liu Y, Qi M, Lu Z, Shi H, Wang J, et al. 2017. Ythdc2 is
674 an N6-methyladenosine binding protein that regulates mammalian spermatogenesis. *Cell*
675 *Res* **27**: 1115–1127.

676 Insco ML, Bailey AS, Kim J, Olivares GH, Wapinski OL, Tam CH, Fuller MT. 2012. A Self-
677 Limiting Switch Based on Translational Control Regulates the Transition from
678 Proliferation to Differentiation in an Adult Stem Cell Lineage. *Cell Stem Cell* **11**: 689–
679 700.

680 Insco ML, Leon A, Tam CH, McKearin DM, Fuller MT. 2009. Accumulation of a differentiation
681 regulator specifies transit amplifying division number in an adult stem cell lineage. *Proc*
682 *Natl Acad Sci U S A* **106**: 22311–6.

683 Ishiguro K ichiro, Matsuura K, Tani N, Takeda N, Usuki S, Yamane M, Sugimoto M, Fujimura
684 S, Hosokawa M, Chuma S, et al. 2020. MEIOSIN Directs the Switch from Mitosis to
685 Meiosis in Mammalian Germ Cells. *Dev Cell* **52**: 429-445.e10.

686 Jain D, Puno MR, Meydan C, Lailler N, Mason CE, Lima CD, Anderson KV, Keeney S. 2018.
687 ketu mutant mice uncover an essential meiotic function for the ancient RNA helicase
688 YTHDC2. *eLife* **7**.

689 Johnson TA, Niedenberger BA, Kirsanov O, Harrington EV, Malachowski T, Geyer CB. 2023.
690 Differential responsiveness of spermatogonia to retinoic acid dictates precocious
691 differentiation but not meiotic entry during steady-state spermatogenesis. *Biol Reprod*
692 **108**: 822–836.

693 Kassir Y, Granot D, Simchen G. 1988. IME1, a positive regulator gene of meiosis in S.
694 cerevisiae. *Cell* **52**: 853–862.

695 Kehoe SM, Oka M, Hankowski KE, Reichert N, Garcia S, McCarrey JR, Gaubatz S, Terada N.
696 2008. A Conserved E2F6-Binding Element in Murine Meiosis-Specific Gene
697 Promoters1. *Biol Reprod* **79**: 921–930.

698 Kimble J. 2011. Molecular regulation of the mitosis/meiosis decision in multicellular organisms.
699 *Cold Spring Harb Perspect Biol* **3**: a002683.

700 Kitamura Y, Uranishi K, Hirasaki M, Nishimoto M, Suzuki A, Okuda A. 2021. Identification of
701 germ cell-specific Mga variant mRNA that promotes meiosis via impediment of a non-
702 canonical PRC1. *Sci Rep* **11**: 9737.

703 Kojima ML, de Rooij DG, Page DC. 2019. Amplification of a broad transcriptional program by a
704 common factor triggers the meiotic cell cycle in mice. *eLife* **8**.

705 Kretschmer J, Rao H, Hackert P, Sloan KE, Höbartner C, Bohnsack MT. 2018. The m6A reader
706 protein YTHDC2 interacts with the small ribosomal subunit and the 5'-3'
707 exoribonuclease XRN1. *RNA N Y N* **24**: 1339–1350.

708 Li L, Krasnykov K, Homolka D, Gos P, Mendel M, Fish RJ, Pandey RR, Pillai RS. 2022. The
709 XRN1-regulated RNA helicase activity of YTHDC2 ensures mouse fertility
710 independently of m6A recognition. *Mol Cell* **82**: 1678-1690.e12.

711 Love MI, Huber W, Anders S. 2014. Moderated estimation of fold change and dispersion for
712 RNA-seq data with DESeq2. *Genome Biol* **15**: 550.

713 Madisen L, Zwingman TA, Sunkin SM, Oh SW, Zariwala HA, Gu H, Ng LL, Palmiter RD,
714 Hawrylycz MJ, Jones AR, et al. 2010. A robust and high-throughput Cre reporting and
715 characterization system for the whole mouse brain. *Nat Neurosci* **13**: 133–140.

716 Maeda I, Okamura D, Tokitake Y, Ikeda M, Kawaguchi H, Mise N, Abe K, Noce T, Okuda A,
717 Matsui Y. 2013. Max is a repressor of germ cell-related gene expression in mouse
718 embryonic stem cells. *Nat Commun* **4**: 1754.

719 Mark M, Jacobs H, Oulad-Abdelghani M, Dennefeld C, Féret B, Vernet N, Codreanu C-A,
720 Chambon P, Ghyselinck NB. 2008. STRA8-deficient spermatocytes initiate, but fail to
721 complete, meiosis and undergo premature chromosome condensation. *J Cell Sci* **121**:
722 3233–3242.

723 Matson CK, Murphy MW, Griswold MD, Yoshida S, Bardwell VJ, Zarkower D. 2010. The
724 Mammalian Doublesex Homolog DMRT1 Is a Transcriptional Gatekeeper that Controls
725 the Mitosis versus Meiosis Decision in Male Germ Cells. *Dev Cell* **19**: 612–624.

726 McKearin DM, Spradling AC. 1990. bag-of-marbles: a Drosophila gene required to initiate both
727 male and female gametogenesis. *Genes Dev* **4**: 2242–51.

728 Nakagawa T, Zhang T, Kushi R, Nakano S, Endo T, Nakagawa M, Yanagihara N, Zarkower D,
729 Nakayama K. 2017. Regulation of mitosis-meiosis transition by the ubiquitin ligase β-
730 TrCP in male germ cells. *Dev Camb Engl* **144**: 4137–4147.

731 Peart NJ, Johnson TA, Lee S, Sears MJ, Yang F, Quesnel-Vallières M, Feng H, Recinos Y,
732 Barash Y, Zhang C, et al. 2022. The germ cell-specific RNA binding protein RBM46 is
733 essential for spermatogonial differentiation in mice ed. W. Yan. *PLoS Genet* **18**:
734 e1010416.

735 Pohlers M, Truss M, Frede U, Scholz A, Strehle M, Kuban R-J, Hoffmann B, Morkel M,
736 Birchmeier C, Hagemeier C. 2005. A Role for E2F6 in the Restriction of Male-Germ-
737 Cell-Specific Gene Expression. *Curr Biol* **15**: 1051–1057.

738 Qian B, Li Y, Yan R, Han S, Bu Z, Gong J, Zheng B, Yuan Z, Ren S, He Q, et al. 2022. RNA
739 binding protein RBM46 regulates mitotic-to-meiotic transition in spermatogenesis. *Sci*
740 *Adv* **8**: eabq2945.

741 Qin J, Wang C, Zhu Y, Su T, Dong L, Huang Y, Hao K. 2021. Mga safeguards embryonic stem
742 cells from acquiring extraembryonic endoderm fates. *Sci Adv* **7**: eabe5689.

743 Qiu X, Hill A, Packer J, Lin D, Ma Y-A, Trapnell C. 2017a. Single-cell mRNA quantification
744 and differential analysis with Census. *Nat Methods* **14**: 309–315.

745 Qiu X, Mao Q, Tang Y, Wang L, Chawla R, Pliner HA, Trapnell C. 2017b. Reversed graph
746 embedding resolves complex single-cell trajectories. *Nat Methods* **14**: 979–982.

747 Romer KA, de Rooij DG, Kojima ML, Page DC. 2018. Isolating mitotic and meiotic germ cells
748 from male mice by developmental synchronization, staging, and sorting. *Dev Biol* **443**:
749 19–34.

750 Saito Y, Hawley BR, Puno MR, Sarathy SN, Lima CD, Jaffrey SR, Darnell RB, Keeney S, Jain
751 D. 2022. YTHDC2 control of gametogenesis requires helicase activity but not m6A
752 binding. *Genes Dev* **36**: 180–194.

753 Smith HE, Su SS, Neigeborn L, Driscoll SE, Mitchell AP. 1990. Role of IME1 expression in
754 regulation of meiosis in Saccharomyces cerevisiae. *Mol Cell Biol* **10**: 6103–6113.

755 Soh YQS, Junker JP, Gill ME, Mueller JL, van Oudenaarden A, Page DC. 2015. A Gene
756 Regulatory Program for Meiotic Prophase in the Fetal Ovary. *PLoS Genet* **11**: e1005531.

757 Soh YQS, Mikedis MM, Kojima M, Godfrey AK, de Rooij DG, Page DC. 2017. Meioc
758 maintains an extended meiotic prophase I in mice ed. P.E. Cohen. *PLoS Genet* **13**:
759 e1006704.

760 Stielow B, Finkernagel F, Stiewe T, Nist A, Suske G. 2018. MGA, L3MBTL2 and E2F6
761 determine genomic binding of the non-canonical Polycomb repressive complex PRC1.6
762 ed. L. Di Croce. *PLOS Genet* **14**: e1007193.

763 Storre J, Elsässer H, Fuchs M, Ullmann D, Livingston DM, Gaubatz S. 2002. Homeotic
764 transformations of the axial skeleton that accompany a targeted deletion of *E2f6*. *EMBO*
765 *Rep* **3**: 695–700.

766 Stuart T, Butler A, Hoffman P, Hafemeister C, Papalexi E, Mauck WM, Hao Y, Stoeckius M,
767 Smibert P, Satija R. 2019. Comprehensive Integration of Single-Cell Data. *Cell* **177**:
768 1888-1902.e21.

769 Suzuki A, Hirasaki M, Hishida T, Wu J, Okamura D, Ueda A, Nishimoto M, Nakachi Y, Mizuno
770 Y, Okazaki Y, et al. 2016. Loss of MAX results in meiotic entry in mouse embryonic and
771 germline stem cells. *Nat Commun* **7**: 11056.

772 Trapnell C, Cacchiarelli D, Grimsby J, Pokharel P, Li S, Morse M, Lennon NJ, Livak KJ,
773 Mikkelsen TS, Rinn JL. 2014. The dynamics and regulators of cell fate decisions are
774 revealed by pseudotemporal ordering of single cells. *Nat Biotechnol* **32**: 381–386.

775 Uranishi K, Hirasaki M, Kitamura Y, Mizuno Y, Nishimoto M, Suzuki A, Okuda A. 2021. Two
776 DNA binding domains of MGA act in combination to suppress ectopic activation of
777 meiosis-related genes in mouse embryonic stem cells. *Stem Cells* **39**: 1435–1446.

778 van Werven FJ, Amon A. 2011. Regulation of entry into gametogenesis. *Philos Trans R Soc B*
779 *Biol Sci* **366**: 3521–3531.

780 Washkowitz AJ, Schall C, Zhang K, Wurst W, Floss T, Mager J, Papaioannou VE. 2015. Mga is
781 essential for the survival of pluripotent cells during peri-implantation development. *Dev*
782 *Camb Engl* **142**: 31–40.

783 Wojtas MN, Pandey RR, Mendel M, Homolka D, Sachidanandam R, Pillai RS. 2017. Regulation
784 of m6A Transcripts by the 3′→5′ RNA Helicase YTHDC2 Is Essential for a Successful
785 Meiotic Program in the Mammalian Germline. *Mol Cell* **68**: 374-387.e12.

786 Yokobayashi S, Liang C-Y, Kohler H, Nestorov P, Liu Z, Vidal M, van Lohuizen M, Roloff TC,
787 Peters AHFM. 2013. PRC1 coordinates timing of sexual differentiation of female
788 primordial germ cells. *Nature* **495**: 236–240.

789